A Motion Planner for Maintaining Landmark Visibility with a Differential Drive Robot

Jean-Bernard Hayet, Claudia Esteves, and Rafael Murrieta-Cid

Abstract This work studies the interaction of the nonholonomic and visibility constraints of a robot that has to maintain visibility of a static landmark. The robot is a differential drive system and has a sensor with limited field of view. We determine the necessary and sufficient conditions for the existence of a path for our system to be able to maintain landmark visibility in the presence of obstacles. We present a complete motion planner that solves this problem based on a recursive subdivision of a path computed for a holonomic robot with the same visibility constraints.

1 Introduction

Landmarks are of common use in robotics, either to localize the robot with respect to them [17] or to navigate in all kinds of environments [3], being used as goals or subgoals to reach or perceive during the motion. Landmarks can be defined in several manners: From single, characteristic image points with useful properties, up to a 3D object associated with a semantic label and having 3D position accuracy [7]. In all cases, this definition involves at some degree properties of saliency and invariance to viewpoint changes.

To use landmarks in the context of mobile robotics, the first basic requirement is to perceive them during the robot motion. It is to this end that our current research efforts are focused on. Although landmarks have been extensively used, this is to our knowledge *the first attempt* to show whether or not a path of a holonomic robot in the

Jean-Bernard Hayet · Rafael Murrieta-Cid
Centro de Investigación en Matemáticas, CIMAT.
Guanajuato, México, e-mail: {jbhayet, murrieta}@cimat.mx

Claudia Esteves
Facultad de Matemáticas de la Universidad de Guanajuato.
Guanajuato, México.
e-mail: cesteves@cimat.mx

presence of obstacles that has to maintain visibility of one landmark with a limited sensor can be transformed into a feasible path for a differential drive robot (DDR). We believe that our research is very pertinent given that a lot of mobile robots are DDRs equipped with limited field of view sensors (e.g., lasers or cameras).

As it is well known in mobile robotics research, nonholonomic systems are characterized by constraint equations involving the time derivatives of the system configuration variables. If the state transition equation is integrable, the corresponding system is said holonomic; otherwise, it is said nonholonomic [10].

From the point of view of motion planning, the main implication of nonholomic constraints is that a collision-free path in the configuration space does not necessarily induce a feasible path for the system. Purely geometric techniques to find collision-free paths do not apply directly here.

1.1 Related work

Motion planning with nonholonomic constraints has been a very active research field (a nice overview is given in [10]). The most important results in this field have been obtained by addressing the problem with tools from differential geometry and control theory. Laumond pioneered this research and produced the result that a free path for a holonomic robot moving among obstacles in a 2D workspace can always be transformed into a feasible path for a nonholonomic car-like robot by making car maneuvers [11]. Recently, a significant amount of work has been done on the problem of planning collision-free paths for nonholonomic systems, for instance, Isler et al. have used the results of the Dubins car to address pursuit-evasion problems [8].

The study of optimal paths for nonholonomic systems has also been an active research topic. Reeds and Shepp determined the shortest paths for a car-like robot that can move forward and backward [14]. In [16] a complete characterization of the shortest paths for a car-like robot is given. In [1], Balkcom and Mason determined the time-optimal trajectories for a DDR using Pontryagin's Maximum Principle (PMP) and geometric analysis. In [4], PMP is used to obtain the extremal trajectories to minimize the amount of wheel rotation for a DDR. In [13], the authors used the curves proposed by [2] in the context of visual servoing. Here, we use similar curves but the fact that our environments are populated with obstacles makes the problem substantially different.

1.2 Contributions

In this paper, we consider the problem of planning paths for a DDR, whose motion is further constrained by sensing considerations and by obstacles in the environment. These constraints generate both, motion and visibility obstructions. We extend our results from previous works [2]. We provide the necessary and sufficient conditions

to compute feasible trajectories for the DDR with *limited sensing capabilities* to maintain landmark visibility in the *presence of obstacles*. Our contributions are:

1. We propose a complete planner to compute collision-free paths for a circular *holonomic* robot maintaining landmark visibility among obstacles.
2. We provide the controls for the execution of the optimal motion primitives.
3. We give the necessary and sufficient conditions for the feasibility of a path for the DDR in the presence of obstacles and with visibility constraints, provided that a collision-free path generated for the *holonomic* system with the same visibility constraints exists.
4. We implement a complete motion planner for the DDR maintaining landmark visibility, based on a recursive subdivision of the holonomic path.

2 Problem settings and approach overview

2.1 The differential drive robot

The DDR is described in Fig. 1. It is controlled through commands to its two wheels, i.e. through angular velocities w_l and w_r. We make the usual assignment of a body-attached $x'y'$ frame to the robot. The origin is at the midpoint between the two wheels, y'-axis parallel to the axle, and the x'-axis pointing forward, parallel to the robot heading. The angle θ is the angle formed by the world x-axis and the robot x'-axis. The robot can move forward and backward. The heading is defined as the direction in which the robot moves, so the heading angle with respect to the robot x-axis is zero (forward move) or π (backward move). The position of the robot w.r.t the origin will be defined either in Cartesian coordinates (x,y) or in polar coordinates $(r,\alpha) : r = \sqrt{x^2+y^2}$, $\alpha = \arctan\frac{y}{x}$. Figure 1 sums up these conventions.

The robot is equipped with a pan-controllable sensor with limited field of view (e.g., a camera), that can move w.r.t. the robot basis. We will suppose that this sensor is placed on the robot so that the optical center always lies directly above the origin of the robot's local coordinate frame, i.e., the center of rotation of the sensor is the same as the one of the robot. Its pan angle ϕ is the angle from the robot x'-axis to its optical axis. The sensor is limited, both in angle and in range: $\phi \in [\phi_1, \phi_2]$ and the robot visibility region is made by the points p such that the Euclidean distance d from p to the robot satisfy $d_{min} \leq d \leq d_{max}$. Notice that the limitation of the sensor induces virtual obstacles in the configuration space even without physical obstacles. We first assume that the robot moves in the absence of physical obstacles, and then remove this assumption in Section 3.

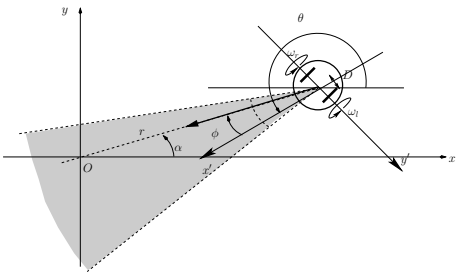

Fig. 1: DDR with visibility constraints. The robot visibility region is depicted in grey (filled region).

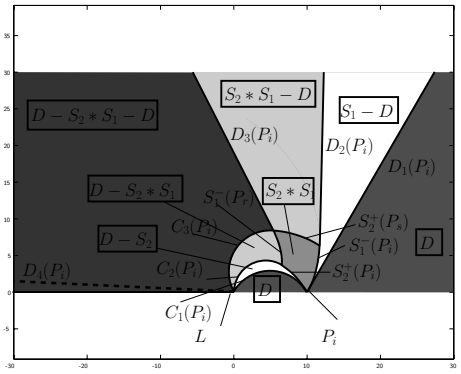

Fig. 2: Distribution of shortest paths, revised from [2] into [6].

2.2 Optimal curves under visibility constraints for a DDR

In [2], it has been shown that the shortest distance paths, in the absence of obstacles for a DDR under *angular constraints only* are composed of three motion primitives: straight-line segments, in-site rotations without translation and logarithmic spirals, i.e. curves for which the camera pan angle is saturated. In [2], a characterization of the shortest paths for the system based on a partition of the plane into disjoint regions was also provided. This characterization (called a synthesis) attempted to obtain the globally optimal paths. Recently in [15], it has been shown that the synthesis presented in [2] was incomplete. Indeed, the work presented in [15] showed a concatenation of motion primitives in which the path is shorter than the one proposed in [2]. Motivated by the work in [15], we have revisited the problem and found the complete partition of the plane (see Fig. 2) and the corresponding globally optimal paths in the absence of obstacles [6]. In that work we showed that the globally optimal paths without obstacles are made of at most seven motion primitives, four (at most) of which produce translation (line-spiral*spiral-line) [1] and three (at most) correspond to in-site rotations. Seven types of trajectories are possible (D, $D-S$, $S-D$, $S-S$, $D-S*S$, $S*S-D$ and $D-S*S-D$). By lack of space, we cannot further develop on this issue in this paper, but the reader is referred to [6] (available on line) for details.

In this paper, we present a complete motion planner for the DDR maintaining landmark visibility in the presence of obstacles, based on a recursive subdivision of the holonomic path. The curves from [2, 6] replace the holonomic path.

[1] In the description of trajectories, "*" means a non-differentiable point, and "-" is a smooth transition point.

2.3 Approach overview

In [11] it has been shown that a free path for a holonomic robot moving among obstacles in a 2D workspace can always be transformed into a free path for a non-holonomic car-like robot. Three necessary and sufficient conditions guarantee the existence of the path for the car-like robot in the presence of obstacles, provided that a path for a holonomic robot exist.

1. The nonholonomic robot must be Small Time Local Controllable (STLC).
2. The existence of obstacles forces the use of some given metric in the plane to measure the robot clearance. Hence, the topology induced by the robot motion primitives metric and the one induced by the metric measuring the distance between the obstacles and the robot must be equivalent.
3. There must be $\varepsilon > 0$ clearance between the robot and the obstacles.

Here, we follow the same methodology presented in [11], that we applied to a DDR equipped with a sensor with a limited range and field of view.

The remaining of this work is organized as follows: In Section 3 we present a complete motion planner for a *holonomic* disk, which generates collision-free paths while maintaining landmark visibility. In Section 4 we show the admissible controls to generate our motion primitives with our state transition equation (system model) and we prove the STLC of our system. In Section 5 we use our motion primitives to determine lower and upper bounds of the paths metric and we show that the topology of the robot motion primitives metric and the metric used to measure the distance between the obstacles and the robot are equivalent. Section 6 presents a motion planner for the DDR able to maintain landmark visibility and simulation results. Finally in Section 7 we present the conclusion and future work.

3 Configuration space induced by visibility constraints

3.1 Configuration space without obstacles

As mentioned above, our robot must maintain visibility of a landmark. By visibility we mean that a clear line of sight, lying within the minimal and maximal bounds of the sensor rotation angle and range, can join the landmark and the sensor. The landmark is static and coincident with the origin O of the coordinate system. The visibility constraints imposed by the landmark can be written as

$$\theta = \alpha - \phi + (2k+1)\pi, k \in \mathbb{Z}, \tag{1}$$

$$\phi_1 \leq \phi \leq \phi_2, \tag{2}$$

$$d_{min} \leq r \leq d_{max}. \tag{3}$$

From these equations, we can describe precisely the robot admissible configuration space $\mathscr{C}_{adm}$. The robot can be seen as living in $SE(2)$, as from Eq. 1, ϕ is not really a degree of freedom. Moreover, Eq. 1 adds a constraint on x, y and θ, that can be rewritten

$$\phi_1 \leq -\theta + \arctan(\frac{y}{x}) + (2k+1)\pi \leq \phi_2 \text{ for some } k \in \mathbb{Z}. \quad (4)$$

This means that the visibility constraint both in range and angle can be translated into virtual obstacles in $SE(2)$. From Eq. 4, it is straightforward to deduce the admissible configuration space, which is $SE(2)$ minus these obstacles. Fig. 3 gives a representation of the virtual obstacle (there is actually only one obstacle) in $SE(2)$ for $\phi_2 = -\phi_1 = \frac{\pi}{2}$ (a) and $\phi_2 = -\phi_1 = \frac{\pi}{3}$ (b), as the hollow volume in $SE(2)$. It is worth noting that the free space resulting from this visibility obstacle is made of one single, helical-shaped component of $SE(2)$, which becomes smaller while the authorized pan range is smaller. We call $\mathscr{C}^{\phi}_{adm}$ the admissible configuration space resulting from the angular constraints 2 and 3.

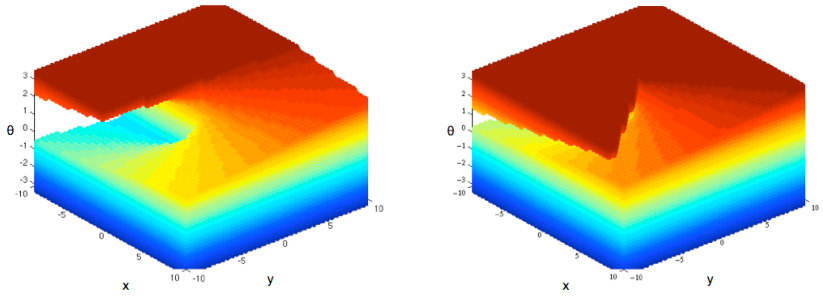

Fig. 3: Admissible configuration space $\mathscr{C}^{\phi}_{adm}$ in the case of a (x, y, θ) configuration space: visibility acts as a virtual obstacle in $SE(2)$. The obstacle is depicted for $(\phi_1, \phi_2) = (-\frac{\pi}{2}, \frac{\pi}{2})$ (left) and $(\phi_1, \phi_2) = (-\frac{\pi}{3}, \frac{\pi}{3})$ (right) .

As far as the range constraints of the inequalities 3 are concerned, they introduce two other virtual cylindrical obstacles which reduce the admissible configuration space into $\mathscr{C}^{r}_{adm}$. Finally the combination of these constraints gives rise to the admissible configuration space :

$$\mathscr{C}_{adm} = \mathscr{C}^{\phi}_{adm} \cap \mathscr{C}^{r}_{adm}.$$

A simpler characterization can be made in the (x, y, ϕ) space, instead of the classical (x, y, θ). These two representations are equivalent, since ϕ and θ are related by Equation 1, and so are the constraints equations, but the admissible configuration space, as depicted on Fig. 4, left, is easier to handle, as the constraints over ϕ (inequalities 2) do not depend on x or y. As a result, in that case, $\mathscr{C}^{\phi}_{adm}$ is simply the space between the two planes $\phi = \phi_1$ and $\phi = \phi_2$, and $\mathscr{C}_{adm}$ is the intersection of this

volume with $\mathscr{C}^r_{adm}$. The advantage of this representation is that it makes easier the task of determining a complete algorithm for the holonomic version of the DDR.

3.2 Finding a path for a holonomic robot with visibility constraints

Let us suppose that our DDR is disk-shaped. We also suppose we are given a holonomic robot with the same circular shape. The holonomic robot evolves in a plane filled with obstacles and has to respect the visibility constraint.

The free space $\mathscr{C}_{free}$ is defined as the set of configurations inside $\mathscr{C}_{adm}$ which (1) are not in collision with the physical obstacles and (2) are not in the shadow areas created by these same obstacles. We can build it on top of $\mathscr{C}_{adm}$ as depicted on Fig. 4, right, by working in its projection on the *xy* plane. To begin with, all the physical obstacles, dilated by the circular robot, are subtracted from $\mathscr{C}_{adm}$. We get, in white, the *collision obstacles*. In a second step, we remove the obstacles shadows w.r.t. the origin. We get, in light gray, the *visibility (virtual) obstacles*. The resulting projection of $\mathscr{C}_{free}$ is the dark gray area, delimited by arcs of circles and straight line segments. Note that the obstacles, and in particular the visibility ones, do not depend on the values of ϕ, so that $\mathscr{C}_{obst}$ is made of cylinders in $SE(2)$, by translating the projection of Fig. 4, right along the ϕ axis.

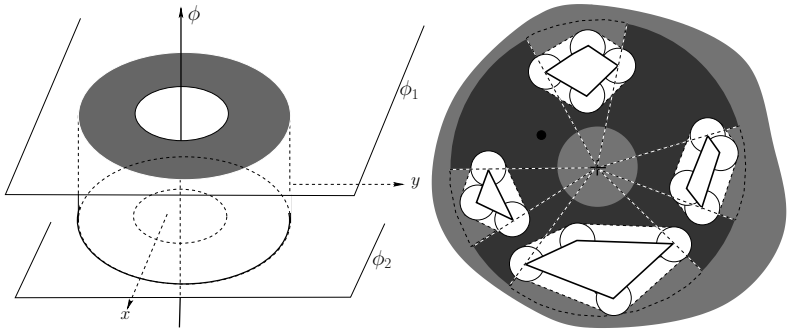

Fig. 4: Left, $\mathscr{C}_{adm}$ for a (x,y,ϕ) configuration space, delimited by two horizontal planes on ϕ and two vertical cylinders. Right, construction of $\mathscr{C}^g_{free}$ for the (x,y,ϕ) representation. By dilating physical obstacles in the *xy* plane to define collision obstacles (white), the circular robot can be reduced to a point (black). Shadows and visibility constraints define visibility obstacles (light gray).

Let $\mathscr{C}^g_{free}$ be the domain in the *xy* plane that generates $\mathscr{C}_{free}$. Several complete algorithms can generate a path for a 2D point in $\mathscr{C}^g_{free}$, e.g. by building a roadmap capturing the domain connectivity [9]. Among them :

- the Generalized Voronoi Graph (GVG) approach. Obstacles here are made of arcs of circles and line segments, hence the GVG is made of arcs of parabola

(circle-line), of hyperbola (circle-circle) and line segments (line-line). This is the approach taken in the simulations of section 6,
- the Visibility Graph approach. It consists in generating a graph connecting all mutually visible points among vertices from the obstacles.

Any of these two approaches gives a complete algorithm for finding a path for a 2D point in $\mathscr{C}^g_{free}$ by connecting the desired start and end points to the generated graph [9]. By using this classical result, we can now state

Theorem 0.1. *The problem of planning a path in $\mathscr{C}_{free} \subset SE(2)$ for a holonomic, circular robot with visibility constraints on both range and angular displacement of its sensor is reductible to the problem of finding a path for a single point in $\mathscr{C}^g_{free} \subset \mathbb{R}^2$.*

Proof. Let $P_i = (x_i, y_i, \theta_i)^T$ and $P_f = (x_f, y_f, \theta_f)^T$ be two free initial and final configurations in $SE(2)$. By construction, the 2D points $(x_i, y_i)^T$ and $(x_f, y_f)^T$ belong to $\mathscr{C}^g_{free}$. Now suppose that we can find a path s^g connecting them in $\mathscr{C}^g_{free}$,

$$\begin{aligned} s^g : [0,1] &\rightarrow \mathscr{C}^g_{free} \\ s^g(0) &= (x_i, y_i)^T, \qquad s^g(1) = (x_f, y_f)^T \\ s^g(t) &= (x(t), y(t))^T. \end{aligned}$$

Then, if ϕ_i and ϕ_f are the sensor angle relative to the robot (given by Eq. 1) at initial and final configurations, let us define:

$$\begin{aligned} s_\theta : [0,1] &\rightarrow SO(2) \\ s_\theta(t) &= \arctan(\tfrac{y(t)}{x(t)}) - (1-t)\phi_i - t\phi_f + \pi. \end{aligned}$$

The function s_θ is continuous on $[0,1]$ since s^g is also continuous and $(x(t), y(t)) \neq (0,0)$. Then we can define the following path in $SE(2)$:

$$\begin{aligned} s : [0,1] &\rightarrow SE(2) \\ s(t) &= (x(t), y(t), s_\theta(t))^T. \end{aligned}$$

The path is continuous, it satisfies the initial and final constraints, and, by construction, as for all $t \in [0,1]$, $(1-t)\phi_i + t\phi_f \in [0, 2\pi)$, it also satisfies the visibility constraints at every point.

Conversely, if we are not able to find any free path in $\mathscr{C}^g_{free}$, we cannot have any free path in $SE(2)$: if there were, its projection on $\mathbb{R}^2$ would also be free, which contradicts our initial assumption. As a consequence, an algorithm that solves the planning problem in $\mathscr{C}^g_{free}$ also solves the problem in $\mathscr{C}_{free}$. □

4 System controls and small time local controlability

We generate a state transition equation with two controls only. In this scheme, we suppose that the sensor is pointing to the landmark by adjusting its angle value

according to equation 1, thus the sensor control is not considered in this motion analysis. It must be determined, whether this system is STLC or not. Far enough from the visibility obstacles, the robot can move forward and backward, hence it is a symmetric system. The construction of the state transition equation is as follows.

First, we get the derivatives $\dot{\phi}$ and $\dot{\alpha}$:

$$\dot{\phi} = \dot{\alpha} - \dot{\theta} \text{ and } \dot{\alpha} = \frac{\dot{y}x - \dot{x}y}{x^2 + y^2}. \tag{5}$$

The linear and angular velocities u_1 and u_2 can be expressed in function of the wheels controls w_l and w_r, as:

$$u_1 = w_r + w_l,\ u_2 = w_r - w_l. \tag{6}$$

Therefore, the state variables are:

$$\dot{\theta} = w_r - w_l,\ \dot{x} = \cos\theta(w_r + w_l) \text{ and } \dot{y} = \sin\theta(w_r + w_l). \tag{7}$$

A key observation is the following: ϕ is not a degree of freedom. It can be expressed as a function of x, y and θ. Hence, the robot configuration is totally defined by (x, y, θ). ϕ and $\dot{\phi}$ are adjusted so that the system maintain landmark visibility.

The derivative $\dot{\phi}$ can be expressed directly in function of the controls u_1, u_2 and the configuration variables (θ, x, y). This can be done by substituting in 5, the values of $\dot{\alpha}$ and $\dot{\theta}$ from Equations 5 and 7,

$$\dot{\phi} = \frac{(y\cos\theta - x\sin\theta)u_1}{x^2 + y^2} - u_2. \tag{8}$$

Therefore, the state transition equation takes the form:

$$\begin{pmatrix} \dot{x} \\ \dot{y} \\ \dot{\theta} \end{pmatrix} = \begin{pmatrix} \cos\theta & 0 \\ \sin\theta & 0 \\ 0 & 1 \end{pmatrix} \begin{pmatrix} u_1 \\ u_2 \end{pmatrix}, \tag{9}$$

which is exactly the same of the differential drive robot[1, 12].

We underline that, the *three only motion primitives* are straight lines, rotation in site and logarithmic spirals [2]. The vector field associated to the straight line is $\overrightarrow{X_1} = (\cos\theta, \sin\theta, 0)^T$, the one associated to the rotation in site is simply $\overrightarrow{X_2} = (0, 0, 1)^T$.

Now let us express the vector field associated to the spirals. The equations of these curves are [2]:

$$r = r_0 e^{(\alpha_0 - \alpha)/\tan\phi}, \tag{10}$$

where (r_0, α_0) is one point of the spiral and ϕ remain constant along it. From the previous equation, and by using (1) the equation $\phi = \alpha - \theta + \pi$ and (2) the relation $\alpha = \arctan\frac{y}{x}$, we can easily derive the corresponding vector field, after some algebraic developments

$$\overrightarrow{X_3} = \begin{pmatrix} -\frac{x^2+y^2}{y-x\tan\theta} \\ -\tan\theta\frac{x^2+y^2}{y-x\tan\theta} \\ 1 \end{pmatrix}. \tag{11}$$

This vector field is not defined for $y = x\tan\theta$, which corresponds to zones where the robot has to follow a straight line. In fact, in that case $\overrightarrow{X_3} = \overrightarrow{X_1}$.

A question that naturally arises is: What are the open-loop controls needed for the robot to follow the logarithmic, saturating sensor pan angle? These controls can be derived from the following. When the robot moves drawing sector of logarithmic spirals, the camera pan angle is saturated and hence the landmark is in the limit of the sensor field of view. Hence, the saturated sensor pan angle, and more generally any trajectory maintaining the sensor pan angle constant, satisfy $\dot{\phi} = 0$.

Now, by using Eq.8, we obtain a relation between u_1 and u_2:

$$(y\cos\theta - x\sin\theta)u_1 = (x^2+y^2)u_2,$$

which can be easily re-written in its polar form

$$u_2 = \frac{1}{r}u_1\sin(\alpha-\theta). \tag{12}$$

In terms of left and right wheels controls, we deduce from Eq.12, for $r > 0$,

$$\begin{cases} w_r = & 1 \\ w_l = & \frac{r-\sin(\alpha-\theta)}{r+\sin(\alpha-\theta)}. \end{cases}$$

Again in terms of u_1 and u_2, and by setting $u_1 = 1$,

$$\begin{cases} u_1 = & 1 \\ u_2 = & \frac{\sin(\alpha-\theta)}{r}. \end{cases}$$

Thus, make our system follow the optimal motion primitives, it is sufficient to consider three admissible pairs of controls (u_1, u_2) that allow to satisfy the visibility constraint and lead the robot to trace these primitives: Straight lines, rotation in site and logarithmic spirals. These controls are respectively

$$\begin{pmatrix} 1 \\ 0 \end{pmatrix}, \begin{pmatrix} 0 \\ 1 \end{pmatrix} \text{ and } \begin{pmatrix} 1 \\ \frac{\sin(\alpha-\theta)}{r} \end{pmatrix}. \tag{13}$$

As shown above, the third control produces a logarithmic spiral, and corresponds to a linear combination of the first two vector fields $\overrightarrow{X_1}$ and $\overrightarrow{X_2}$,

$$\overrightarrow{X_3} = a_1\overrightarrow{X_1} + a_2\overrightarrow{X_2} \text{ where } a_i \in \mathbb{R}. \tag{14}$$

Hence, the state transition equation presented in 9 can be used to model our system and trace our motion primitives, and therefore our system is STLC by using Chow theorem [10, 5, 12].

The Lie bracket operation computed over vector files $\overrightarrow{X_1}$ and $\overrightarrow{X_2}$ is $(\sin\theta, -\cos\theta, 0)^T$. It is immediate to see that this new vector field is linearly independent from $\overrightarrow{X_1}$ and $\overrightarrow{X_2}$. Hence, this system is small time locally controllable everywhere in the open of the free space.

Note that the first two controls are constant and therefore bounded, and the third one is also bounded since we consider $r > d_{min} > 0$.

5 Analysis of the metric induced by shortest paths

Let us prove that the metric induced by the total lengths along the shortest paths defined by optimal primitives under visibility constraints is locally equivalent to the Euclidean metric in $\mathbb{R}^2$. Let $(x_i, y_i)^T$ and $(x_f, y_f)^T$ be a pair of initial and final points in the free space. As recorded in 2.2, there are seven kinds of shortest paths: line segments (on which the length is obviously equal to the Euclidean distance in $\mathbb{R}^2$), and four concatenations of one or two line segments with one or two logarithmic spiral at saturated ϕ. Examples of S*S curves, S-D curves, D-S*S curves, and D-S*S-D curves are depicted in Fig. 5. An important consideration is that, as it is shown in [6], if the families of $3-$ and $4-$letter trajectories (e.g. D-S*S) give the optimal path for some configuration (P_i, P_f) then they are either shorter than the $D-S$ (or $S-D$) path, or shorter than the $S-S$ path (which are just instantiations of these families). As a consequence, we can simply focus on the lengths d_{DS} and d_{SS}.

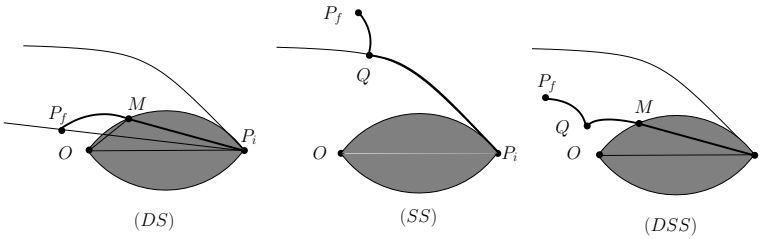

Fig. 5: Some of the shortest paths: concatenation of a line and a ϕ_2 spiral (DS, left), concatenation of a ϕ_2 and a ϕ_1 spiral (SS, center), and concatenation of line and two spirals (DSS, right).

First note that the length of an arc on a logarithmic spiral keeping ϕ constant, starting from a point $P_0 = (r_0, \alpha_0)^T$ and reaching a point $P_1 = (r_1, \alpha_1)^T$ is

$$l_\phi(P_0, P_1) = \frac{r_0}{\cos\phi} |1 - e^{\frac{\alpha_0 - \alpha_1}{\tan\phi}}|. \tag{15}$$

Also note that since $r \geq d_{min} > 0$, whenever P_1 is close enough to P_0,

$$l_\phi(P_0,P_1) \leq \frac{3r_0}{2|\sin\phi|}|\alpha_0-\alpha_1| \leq \frac{9r_0}{4|\sin\phi|}|\sin(\alpha_0-\alpha_1)| \leq \frac{9\|P_0P_1\|}{4|\sin\phi|}. \quad (16)$$

Case of a line segment and a spiral (DS). In that case (Fig. 5, left), the distance between P_i and P_f is given by

$$d_{DS}(P_i,P_f) = \|P_iM\| + l_{\phi_1}(M,P_f).$$

Now note that if P_f is close enough to P_i, by using the bound 16, we get

$$d_{DS}(P_i,P_f) \leq \|P_iM\| + \frac{9}{4|\sin\phi_2|}\|MP_f\| \leq (1+\frac{9}{4|\sin\phi_2|})(\|P_iM\|+\|MP_f\|).$$

Now an analysis of points O, P_i, P_f and M shows that $\frac{\pi}{2} < \pi-\phi_2 < \angle P_fMP_i < \pi$ (with $\phi_2 > 0$) so that $-1 < \cos(P_fMP_i) < -\cos\phi_2$. From the cosine rule in the triangle P_iMP_f, we derive

$$\|P_iM\|^2 + \|MP_f\|^2 + 2\cos\phi_2\|P_iM\|\|MP_f\| \leq \|P_iP_f\|^2,$$

which induces $\|P_iM\| + \|MP_f\| \leq \frac{1}{\sqrt{\cos\phi_2}}\|P_iP_f\|$. Combining this result with the equation above, we have a relation of local equivalence between distances, for $\phi_2 < \frac{\pi}{2}$,

$$\|P_iP_f\| \leq d_{DS}(P_i,P_f) \leq \frac{1}{\sqrt{\cos\phi_2}}(1+\frac{9}{4|\sin\phi_2|})\|P_iP_f\|. \quad (17)$$

Case of two spirals (SS). By using the Equation 15 twice on the two spirals (Fig. 5, center), and with $t_1 = \tan\phi_1, t_2 = \tan\phi_2$,

$$\begin{aligned} d_{SS}(P_i,P_f) = & \quad l_{\phi_2}(P_i,Q) + l_{\phi_1}(Q,P_f) \\ = & \frac{r_{P_i}}{\cos\phi_2}(1-e^{\frac{\alpha_{P_i}-\alpha_Q}{t_2}}) + \frac{r_{P_f}}{\cos\phi_1}(1-e^{\frac{\alpha_{P_f}-\alpha_Q}{t_1}}). \end{aligned}$$

The intersection point Q between the spirals can be easily shown to be

$$\alpha_Q = \frac{t_1t_2}{t_1-t_2}\log\frac{r_{P_i}}{r_{P_f}} + \frac{t_1}{t_1-t_2}\alpha_{P_i} - \frac{t_2}{t_1-t_2}\alpha_{P_f},$$

which can be plugged into the previous equation to give, after simplifications,

$$d_{SS}(P_i,P_f) = a_2r_{P_i} + a_1r_{P_f} - (a_1+a_2)e^{\frac{\alpha_{P_f}-\alpha_{P_i}}{t_1-t_2}}r_{P_i}^{\gamma}r_{P_f}^{1-\gamma},$$

where $a_l = \frac{1}{\cos\phi_l}$ for $l = 1,2$ and $\gamma = \frac{-t_2}{t_1-t_2}$.

Whenever P_f is sufficiently close to P_i (which we will suppose on the x-axis), by using Taylor expansion around P_i,

$$d_{SS}(P_i,P_f) \approx K_x|x_{P_i}-x_{P_f}| + K_y|y_{P_i}-y_{P_f}|,$$

where $K_x = \frac{\sin\phi_2+\sin\phi_1}{\sin(\phi_2+\phi_1)} > 0$ and $K_y = \frac{a_1+a_2}{t_2-t_1}$. It is then straightforward to get, for some other positive constant K'

$$\|P_iP_f\| \leq d_{SS}(P_i,P_f) \leq K'\|P_iP_f\|. \tag{18}$$

Note that in both cases involving spirals, the condition $r \geq d_{min} > 0$ is important to get a neighborhood size that is independent of point P_i. As a consequence, we can state that for any neighborhood of a point P_i in $\mathscr{C}^g_{free}$, there is a smaller neighborhood around P_i such that all the points in this neighborhood can be attained from P_i by the shortest paths of the DDR under visibility constraints that we get from the synthesis of [6]. We can now state the following theorem:

Theorem 0.2. *If a collision-free path for a holonomic robot that maintains visibility of a landmark exists, then, a feasible collision-free path for a DDR with the same visibility constraints also exists, provided that it moves only along the paths composed with the three motion primitives.*

Proof. This theorem is proven given the three properties already shown: (1) The system is STLC, then it can locally maneuver in a neighborhood of the open space. (2) Our motion primitives can be executed with a bounded control and (3) The metric of the primitives induce the same topology and are locally equivalent to the euclidean metric in $\mathbb{R}^2$, from this it follows that the holonomic paths can be always divided and replaced by paths composed of the three motion primitives. □

6 Motion planner and simulations

Here, the results from the previous section are used to propose a complete planner for a circular-shaped DDR navigating among obstacles and having to maintain a landmark in sight, whereas its sensor is under range and angular constraints. Inspired from the classical roadmap-based approach, we implemented a simple planning algorithm according to the following steps :

1. Build $\mathscr{C}^g_{obst} = \overline{\mathscr{C}^g_{free}}$ by taking the union of the dilated obstacles with the shadows induced by the landmark visibility;
2. Build the GVG on $\mathscr{C}^g_{free}$; as $\mathscr{C}^g_{free}$ is made of line segments and arcs of circle, the resulting Voronoi Diagram is made of line segments and arcs of parabola or hyperbola; the graph edges weights are a combination of the edge lengths and of the minimal clearance along this edge, so as to find a compromise between shortest and clearest paths;
3. Given a starting and a goal configurations, compute a path $\hat{s}$ for the holonomic system associated to the robot by connecting these locations to the GVG; if not possible, no non-holonomic path can be found as well;
4. Recursively try to connect the starting and ending points with the optimal primitives of section 2.2; whenever the sub-paths induced by these primitives are in collision, use as a sub-goal the point at middle-path in $\hat{s}$ and apply the recursive procedure to the two resulting pairs of points.

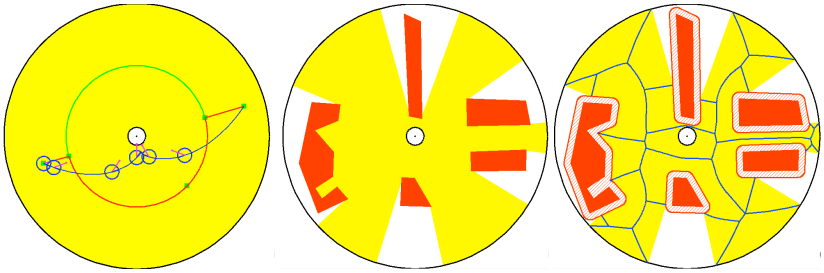

Fig. 6: (Left) Shortest paths for a DDR under visibility constraints alone (angular and distance ranges, represented by the inner and outer circles). The robot shape, heading, and gaze are drawn here, and then omitted for the sake of readability. The Voronoi-based path is in dark, so is the final computed path. (Center) Obstacles (dark) and regions visible from the landmark (light gray). (Right) Construction of $\mathscr{C}^g_{free}$: dilated obstacles (dashed grey) are removed from the visible area and underlying GVG.

Figures 6 (center) and (right) illustrate the first two steps of the algorithm (up to the construction of the GVG), whereas in (left), in the free space, a curve composed of two spirals and in-site rotations is shown. Figure 7 (left) shows an example of path planning among obstacles, all made of concatenations of line segments, in-site rotations and logarithmic spirals. Finally, Figures 7 (center) and (right) illustrate the behavior of the algorithm in narrow passages, where a large number of maneuvers may have to be done to connect the starting and ending points.

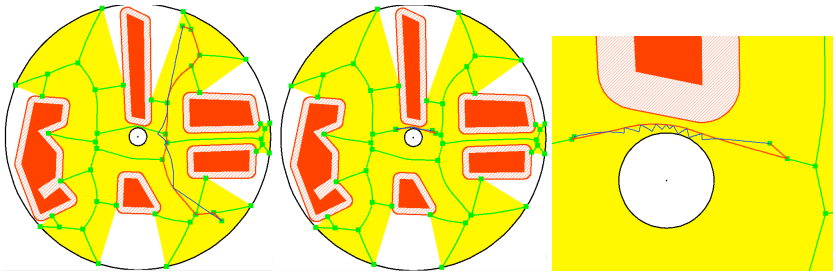

Fig. 7: (Left) Examples of a path computed by the recursive algorithm. (Center) and (Right) Behavior of the planner in narrow passages: as expected, a solution may imply a quantity of maneuvers to finally reach the goal. (Right) is a zoomed view of (Center).

Based on the metrics equivalence, we can ensure the convergence of the recursive algorithm, i.e., whenever a holonomic path exists, we obtain a path for the non-holonomic robot (DDR) after a *finite* number of iterations.

7 Conclusions and future work

In this work, we have proposed a complete motion planner to compute collision-free paths for a holonomic disk robot able to maintain landmark visibility in the presence

of obstacles. We have shown that if a path exist for the holonomic robot then a feasible (collision free and maintaining landmark visibility) path composed by our three motion primitives shall always exist for the DDR. We have also provided the motion controls to execute these motion primitives. Finally, we have implemented a motion planner for the DDR based on a recursive sub-division of the holonomic path. In our planner the motion primitives replace the sections of the holonomic path. As future work, we would like to study the problem of determining a path as sequence of sub-goals defined by several landmarks. In the scheme at least one landmark should be visible at every element of the motion sequence.

References

1. D. Balkcom and M. Mason. Time optimal trajectories for bounded velocity differential drive vehicles. *Int. J. of Robotics Research*, 21(3):199–217, 2002.
2. S. Bhattacharya, R. Murrieta-Cid, and S. Hutchinson. Optimal paths for landmark-based navigation by differential-drive vehicles with field-of-view constraints. *IEEE Trans. on Robotics*, 23(1):47–59, 2007.
3. A. Briggs, C. Detweiler, D. Scharstein, and A. Vandenberg-Rodes. Expected shortest paths for landmark-based robot navigation. *Int. J. of Robotics Research*, 8(12), 2004.
4. H. Chitsaz, S. LaValle, D. Balkcom, and M. Mason. Minimum wheel-rotation paths for differential-drive robots. In *IEEE Int. Conf. on Robotics and Automation*, 2006.
5. H. Choset, K. Lynch, S. Hutchinson, G. Cantor, W. Burgard, L. Kavraki, and S. Thrun. *Principles of Robot Motion: Theory, Algorithms, and Implementations*. MIT Press, Boston, 2005.
6. J. B. Hayet, C. Esteves, and R. Murrieta-Cid. Shortest paths for differential drive robots under visibility and sensor constraints. Technical Report I-09-02/24-02-2009, CIMAT, 2009, Submitted to IEEE-TRO. http://www.cimat.mx/~jbhayet/PUBLIS/Hayet-TR2009.pdf.
7. J. B. Hayet, F. Lerasle, and M. Devy. A visual landmark framework for mobile robot navigation. *Image and Vision Computing*, 8(25):1341–1351, 2007.
8. V. Isler, D. Sun, and S. Sastry. Roadmap based pursuit-evasion and collision avoidance. In *Robot-Sci. Syst*, pages 257–264, 2005.
9. J.-C. Latombe. *Robot motion planning*. Kluwer, 1991.
10. J.-P. Laumond. *Robot motion planning and control*. Springer, 1998.
11. J.-P. Laumond, P. E. Jacobs, M. Taïx, and R. M. Murray. A motion planner for nonholonomic mobile robots. *IEEE Trans. on Robotics and Automation*, 10(5):577–593, 1994.
12. S. LaValle. *Planning Algorithms*. Cambridge University Press, 2006.
13. G. López-Nicolás, S. Bhattacharya, J. Guerrero, C. Sagüés, and S. Hutchinson. Switched homography-based visual control of differential drive vehicles with field-of-view constraints. In *Proc. of the IEEE Int. Conference on Robotics and Automation*, pages 4238–4244, 2007.
14. J. Reeds and L. Shepp. Optimal paths for a car that goes both forwards and backwards. *Pacific J. of Mathematics*, 145(2):367–393, 1990.
15. P. Salaris, F. Belo, D. Fontanelli, L. Greco, and A. Bicchi. Optimal paths in a constrained image plane for purely image-based parking. In *Proc. of the IEEE/RSJ Int. Conf. on Intelligent Robots and Systems*, pages 1673–1680, 2008.
16. P. Souères and J.-P. Laumond. Shortest paths synthesis for a car-like robot. *IEEE Trans. on Automatic Control*, 41(5):672–688, May 1996.
17. S. Thrun. Bayesian landmark learning for mobile robot localization. *Machine Learning*, 33(1), 1998.